Polymer Degradation and Stability 245 (2026) 111858

Contents lists available at ScienceDirect

Polymer Degradation and Stability

journal homepage: www.journals.elsevier.com/polymer-degradation-and-stability

Flame retarded recycled PET foams: Comparative analysis of gas-phase and solid-phase additive performance and feasibility

Kata Enikő Decsov [a], Emese Győry-Slezák [a,b], Dániel Gere [c], Ferenc Ronkay [b,d], Béla Botond Marosfői [e], Sándor Lenk [f], Katalin Bocz [a,*]

[a] Department of Organic Chemistry and Technology, Faculty of Chemical Technology and Biotechnology, Budapest University of Technology and Economics, Műegyetem rkp. 3., H-1111 Budapest, Hungary
[b] Imsys Ltd, Material Testing Laboratory, Mozaik Street 14/A., H-1033 Budapest, Hungary
[c] Department of Polymer Engineering, Faculty of Mechanical Engineering, Budapest University of Technology and Economics, Műegyetem rkp. 3., H-1111 Budapest, Hungary
[d] Jászberény Campus, Eszterházy Károly Catholic University, Eszterházy Square 1, H-3300 Eger, Hungary
[e] Furukawa Electric Institute of Technology Ltd, 1158, Késmárk street. 28/A., Budapest, Hungary
[f] Department of Atomic Physics, Institute of Physics, Budapest University of Technology and Economics, Műegyetem rkp 3., H-1111 Budapest, Hungary

ARTICLE INFO

Keywords:
Poly(ethylene terephthalate)
Recycling
Foaming
Phosphorus flame retardants

ABSTRACT

This study evaluates flame retardant formulations in recycled poly(ethylene terephthalate) (rPET) foams, focusing on processability, performance, and structure-property relationships. Microcellular foams were produced from post-industrial rPET using a CO_2-assisted batch foaming process, incorporating aluminium-tris-(diethylphosphinate) (AlPi), melamine polyphosphate (MPP), and their combination at 5 wt% loading. Morphological, thermal, flammability, mechanical, and optical properties were comprehensively assessed.

The CO_2-assisted process enabled the preparation of highly porous foams (void fraction >70 %) with fine cellular structures (average cell size ~ 2 μm). AlPi showed superior flame retardant performance, achieving a limiting oxygen index (LOI) of 25.0 %, delayed ignition, and a 23 % reduction in peak heat release rate during cone calorimetry. Enhanced char formation containing thermally stable aluminium phosphates was confirmed via energy dispersive spectroscopy (EDS) and attenuated total reflectance infrared spectroscopy (ATR-IR) analyses. In contrast, MPP alone provided limited flame retardancy, and its combination with AlPi offered no synergistic benefit.

Mechanical performance was primarily determined by foam density, with negligible influence of flame retardant additives. The foams exhibited high crystallinity ($\chi > 31$ %) due to strain-induced crystallisation during cell growth, contributing to enhanced thermomechanical stability. Additionally, the microcellular structure enabled excellent optical reflectivity (>90 %) in the visible spectrum, which was retained even in flame-retarded formulations.

1. Introduction

Poly(ethylene terephthalate) (PET) foams offer a wide variety of benefits, such as lightweight and insulation properties, moisture and chemical resistance, mechanical strength, good adhesion properties, thermal stability, durability, and recyclability, which make them versatile and high-performance materials for various demanding applications, including packaging, construction, transportation, and aerospace. Manufacturing foams from recycled PET (rPET), derived from post-consumer or post-industrial packaging PET plastic waste, is an increasingly popular and sustainable option. It reduces environmental impact by lowering plastic waste and the need for virgin materials while cutting costs, as it retains many of the advantageous properties of virgin PET foams. However, foaming recycled PET presents challenges such as polymer degradation, reduced chain entanglement [1] and inconsistent melt flow [2]. These issues can be addressed by strategies like blending with virgin PET, adding processing aids [3], optimizing processing conditions [4], and utilizing advanced foaming techniques [5], ultimately improving foam quality and consistency in rPET foaming applications.

* Corresponding author.
E-mail address: bocz.katalin@vbk.bme.hu (K. Bocz).

https://doi.org/10.1016/j.polymdegradstab.2025.111858
Received 23 July 2025; Received in revised form 21 November 2025; Accepted 10 December 2025
Available online 11 December 2025

The PET foam market is growing in industries that increasingly demand materials capable of meeting stringent fire safety standards (e.g., ASTM E84, EN 13501–1, or International Maritime Organization (IMO) certifications). Enhancing the resistance of recycled PET foams to ignition and fire spread enables manufacturers to comply with regulatory requirements, improve safety, and expand the use of recycled material in high-risk industries.

While many commercially available flame retardant systems for thermoplastic polyesters still rely on halogen-containing additives and synergists, recent research has focused on halogen-free solutions, particularly those based on phosphorus [6]. The mode of action of phosphorus—either through flame inhibition in the gas phase or char formation in the solid phase—depends primarily on its oxidation state [7]. Generally, higher oxidation states of phosphorus lead to greater formation of thermally stable residues and reduced release of phosphorus-containing volatiles [8]. Polymer materials with different surface-to-volume ratios require different flame retardant mechanisms, specifically in condensed-phase and gas-phase activity [9]. Nonetheless, the phosphorus flame retardants for PET foams must possess high thermal stability, capable of withstanding temperatures up to 280 °C during processing, and should not significantly affect melt viscosity, foam density, and mechanical performance. From these considerations, aluminium-tris-(diethylphosphinate) (AlPi), primarily known for its activity in the gas phase but also exhibiting condensed-phase activity [10–12], and melamine polyphosphate (MPP), an effective flame retardant in both the gaseous and condensed phases [13], emerge as suitable phosphorous flame retardant candidates for PET foams. *Ramani* and *Dahoe* [14] reported that in polycaprolactam composites, the combination of AlPi and MPP enhances flame retardant performance, which can be further improved by incorporating organically modified montmorillonite (MMT) nanoclay, providing an effective condesed-phase shielding effect. Similar beneficial interactions between AlPi and MMT nanoclays have also been observed in polylactide [15] and in glass fibre reinforced poly(butylene terephthalate) composites [16]. Nevertheless, as emphasized in a recent study by *Tabaka and Schartel* [17], the fire performance of advanced materials should be optimized in conjunction with other factors, including processability and mechanical performance.

Bethke et al. [18] compared the effect of a phosphonate/phosphate (6H-dibenz[c,e] [1,2]oxaphosphorin,6-[(1-oxido-2,6,7-trioxa-1-phosphabicyclo[2.2.2]oct-4-yl)methoxy]-, 6-oxide (DOP)), a phosphonate (pentaerythritol spirobis(methylphosphonate) (PSMP)), and a phosphinate salt (zinc diethyl phosphinate (DEPZn)) in foams prepared by carbon dioxide (CO_2)-assisted extrusion from bottle-grade PET. In the cone calorimeter test, PSMP, predominantly active in the gas phase, showed the best fire retardant performance (longest time to ignition (TTI) and lowest peak heat release rate (pHRR)). However, PSMP was found to be less suitable for PET, as it caused noticeable chain degradation in the PET matrix, accompanied by processing fluctuations. In terms of processability, the amount of this additive was found to be limited to a maximum of 2 wt%. *Bocz* et al. [19] observed that the porosity of recycled PET foams produced via supercritical CO_2-aided extrusion decreased with increasing aluminium-tris-(diethylphosphinate) (AlPi)-type flame retardant (FR) content. This effect was attributed to the reduced chain length of the recycled polymer matrix and the limited interaction between the polymer and the filler, which may result in a greater number of interfacial defects that facilitate gas escape and hinder expansion. *Lukács* et al. [20] demonstrated that batch foaming enables the production of flame-retarded recycled PET foams with finer and more uniform cell structures—characterised by significantly smaller cell diameters (5–20 μm) and higher cell densities—compared to extrusion foaming, which results in much larger cell diameters (80–500 μm). However, incorporating the AlPi/montmorillonite (MMT) flame-retardant system into the batch foams also resulted in a less uniform foam structure, as indicated by a broader cell size distribution. This irregularity was attributed to debonding at the filler-matrix interphase and the formation of micro holes, which facilitated the gas escape. Notably, the formation of a small number of large-volume cells, which significantly influenced the average cell diameter, was found to be primarily located around the FR particles.

It is also noteworthy that not only do the FR additives affect the foaming behaviour, but the foaming process also affects the fire performance of the polymeric system. Several research studies have shown that after foaming, the limiting oxygen index (LOI) of polymer composites significantly decreases [19–23]. The increased flammability is mainly due to the enlarged interfacial area between the polymer matrix and the surrounding air, as well as the reduced volume concentration of flame retardants in the expanded foam structures. In the condensed phase, the porous foam structure can limit the ability of flame retardants to form a continuous protective char layer to suppress combustion effectively. In research studies, the combustion residues of flame-retarded polylactic acid (PLA) foams [21,23] were found to be porous and fractured, with lower density and uniformity compared to their corresponding bulk composites, which resulted in the shrinkage of foamed samples during combustion. Similarly, the char-promoting efficiency of mineral clays was observed to be limited in highly porous recycled PET foams compared to their bulk counterparts [19,20]. According to *Bocz* et al. [19], the AlPi/MMT system showed more pronounced condensed-phase activity in recycled PET bulk materials than in extrusion foamed samples, as the same additive concentration led to a greater reduction in total heat release (THR) in bulk samples. In contrast, the applied system proved to be more effective in increasing the TTI and reducing the pHRR of the foamed rPET samples compared to the bulk counterparts. *Bethke* et al. [18] further noted that foamed PET samples, obtained by foam extrusion process, required a lower amount of FR to achieve measurable fire retardant efficiency according to the cone calorimeter test, which was attributed to the thermal insulating properties of the porous foam structure.

This research study aims to comprehensively evaluate the feasibility of incorporating phosphorus-based flame retardant formulations into recycled PET foams manufactured via a CO_2-assisted batch process, by assessing not only their flame retardant performance but also their overall influence on processability and on the physical, thermal, mechanical, and optical characteristics. As the structure of the foams is sensitive to the quantity and quality of the components, the additive proportion was kept as low as possible. AlPi and MPP were evaluated individually and in combination to analyse their potential beneficial interactions, with the total amount of flame retardants maintained at 5 wt%.

2. Experimental

2.1. Materials

In this work, post-industrial PET waste (flakes from PET trays) was received from Pro-Form Kft. (Hungary) with an intrinsic viscosity value (IV) of 0.61 ± 0.02 dL/g, was used as recycled PET. As a chain extender (CE), CESA-extend NCA0025531-ZA (Clariant AG, Switzerland) was used. Two types of FR additives, aluminium-tris-(diethylphosphinate) (AlPi), with a phosphorus content of 23.3–24.0 wt% and particle size of 25–50 μm, purchased as Exolit OP1240 from Clariant AG (Switzerland), and melamine polyphosphate (MPP), with a phosphorus content of 12.0–14.0 wt% and particle size of 8–20 μm, purchased as BUDIT® 341 from Budenheim GmbH (Germany), were used, respectively. Cloisite 116-type natural montmorillonite (MMT) (Byk-Chemie GmbH, Germany) was a co-additive.

2.2. Sample preparation

Four types of rPET materials with compositions presented in Table 1 were compounded by a Labtech Scientific LTE 26–44-type twin-screw extruder (Labtech Engineering Co., Thailand) with zone temperatures

Table 1
Composition of the manufactured rPET materials.

Sample	rPET [wt%]	CE [wt%]	MMT [wt%]	AlPi [wt%]	MPP [wt%]	P content [%]
rPET/CE/MMT	97.0	2.0	1.0	-	-	-
rPET/CE/MMT/AlPi	92.0	2.0	1.0	5.0	-	1.2
rPET/CE/MMT/MPP	92.0	2.0	1.0	-	5.0	0.7
rPET/CE/MMT/AlPi/MPP	92.0	2.0	1.0	2.5	2.5	0.9

between 245 and 260 °C. In each composition, 2 wt% CE was used to increase melt strength, while 1 wt% MMT was added to serve as both a nucleating agent and potential flame retardant synergist besides phosphorus-containing additives, as proposed by our previous research works [19,20,24]. Before processing, rPET flakes were dried at 160 °C for 4 h.

The obtained granules were dried again at 160 °C, and then 250 mm wide films with a nominal thickness of 350 μm were manufactured on a Labtech Scientific LRC300 type flat film line (Labtech Engineering Co., Thailand) with a temperature profile of 245/250/255/260/260 °C.

Foamed samples were produced using the following method; rPET films were saturated with CO_2 in a high-pressure vessel (8 cm in diameter) at 60 bar for 48 h. After depressurization, the samples were stored in a freezer at −18 °C to minimize the CO_2 diffusion loss before the foaming step. Then, the high-temperature foaming was performed in a drying oven at 220 °C for 90 s in all cases, during which cell nucleation and growth occurred.

2.3. Characterisation of samples

2.3.1. Scanning electron microscopy (SEM)

The cell structure and morphology of the foamed PET samples were examined using a JEOL JSM-6380LA scanning electron microscope (JEOL Ltd., Japan). Before imaging, the sample surfaces were sputter-coated with a thin gold layer. SEM imaging was conducted at an accelerating voltage of 10.0 kV with a magnification of 200× .

The cell-size distribution was determined from SEM images, based on 1000–1200 measurements per sample. The mean and standard deviation of the cell cross-section diameters were calculated. From these measurements, two different weighted averages of cell size were derived [25]:

The number-weighted mean diameter d_1 was calculated from the sum of the measured diameters divided by the number of measured cells N:

$$d_1 = \frac{\sum_{i=1}^{N} d_i}{N} \tag{1}$$

The diameter of a sphere with a volume equal to the mean cell volume d_2 was calculated using the following formula:

$$d_2 = \left(\frac{\sum_{i=1}^{N} d_i^3}{N}\right)^{1/3} \tag{2}$$

The polydispersity degree (PD) was calculated as the ratio of d_1 and d_2.

Cell density (N_0) was determined based on the SEM images as:

$$N_0 = \left(\frac{n}{A}\right)^{32} \tag{3}$$

where n is the number of cells and A is the area (cm^2).

2.3.2. Density measurement

The mass densities of the foamed samples were measured using Archimedes' Buoyancy test method according to ASTM D792–20. The expansion ratio was defined as the ratio of the bulk material density to that of the foamed material for each composition. Porosity (or void fraction) was calculated as follows:

$$V_f = 100 \times \left(1 - \frac{\rho_{foam}}{\rho_{bulk}}\right) \tag{4}$$

2.3.3. Differential scanning calorimetry (DSC)

Thermal analysis was performed using a DSC131 EVO-type differential scanning calorimeter (Setaram, France) under nitrogen atmosphere. Samples weighing 5–8 were heated from 30 °C to 320 °C at 20 °C/min. The crystallinity (CRF) of each specimen was calculated from the crystallization enthalpy using the following equation:

$$\mathrm{CRF} = \frac{\Delta H_m - \Delta H_{cc}}{\Delta H_m^0 \times (1-\alpha)} \times 100\ [\%] \tag{5}$$

where CRF is the crystalline fraction [%], ΔH_m is the crystal melting enthalpy [J/g], ΔH_{cc} is the cold crystallization enthalpy [J/g], ΔH_m^0 is the specific melting enthalpy of the 100 % crystalline PET, which is 140 [J/g] [26] and α is the ratio of additives [-].

2.3.4. Dynamic mechanical analysis (DMA)

DMA tests were performed using a Q800 apparatus (TA Instruments, USA) in single-frequency-strain mode. Sample dimension were: 25 mm length, 10 mm clamped length, 6 mm width, and ca. 0.5 mm thickness. An oscillation frequency of 1.00 Hz and an oscillation amplitude of 0.1 % were applied, with a static load of 1 N and a 125 % force track, while temperature was varied between room temperature (RT) and 220 °C with a heating rate of 3 °C/min.

2.3.5. Thermogravimetric analysis (TGA)

TGA measurements were performed using a Q5000-type instrument (TA Instruments, USA) in a temperature range of 35–800 °C at a heating rate of 10 °C/min under nitrogen gas flow (25 ml/min). The mass of the samples was between 5–8 mg. The following parameters were determined from the TGA curves: 5 % weight loss temperature: The temperature at which the sample lost 5 % of its initial mass, indicating the onset of significant thermal degradation. Maximum degradation speed: The peak rate of weight loss, determined from the derivative thermogravimetric (DTG) curve. Temperature of maximum degradation speed: The temperature corresponding to the maximum degradation speed. Residue at 600 °C: The remaining mass percentage after heating to 600 °C, represents the char yield and thermal stability.

2.3.6. Limiting oxygen index (LOI)

Limiting oxygen index (LOI) values were measured with a Fire Testing Technology Oxygen Index instrument (Fire Testing Technology, United Kingdom). The foam samples were tested in the test specimen form V, with 140 mm length and 52 mm width, according to ISO 4589–2:2017 standard.

2.3.7. Pyrolysis combustion flow calorimetry (PCFC)

PCFC measurements were carried out on a FAA Micro Calorimeter-type instrument (Fire Testing Technology, United Kingdom) In these measurements the heating rate was 1 °C/*sec*, the combustion temperature was 900 °C, and the maximum pyrolysis temperature was 750 °C. Approximately 5 mg of sample was used in each test, with an oxygen-to-nitrogen flow ratio of about 20:80. From the gained experimental data,

the Fire Growth Capacity (FGC) parameter was calculated following the method described by *Lyon* et al. [27].

2.3.8. Cone calorimetry (CC)

CC tests were carried out using a TCC 918-type instrument (Netzsch, Germany). Four layers of each type of foamed rPET film (sample size 100 × 100 mm, nominal thickness 3 mm, mass 14–16 g) were exposed to a constant heat flux of 35 kW/m^2 from the cone calorimeter at a distance of 25 mm. The main combustion characteristics, such as the heat release rate (HRR), the time to ignition (TTI), mass loss rate (MLR), and smoke production rate (SPR) were measured. From these data, the total heat release (THR), the peak of heat release rate (pHRR), total smoke production (TSP), the residual mass, and the maximum average rate of heat emission (MARHE) were calculated. The measurements were performed in duplicate, where the pHRR values were reproducible within ±10 % while THR values were within ±5 %.

Quantitative analysis of cone calorimeter data was carried out; flame retardance index (FRI) was calculated according to the method proposed by *Vahabi* et al. [28], while flame inhibition effect, barrier and protective effect, and charring effect were calculated using the formulas proposed by *Yan* et al. [29].

2.3.9. SEM-EDS

SEM combined with energy dispersive spectroscopy (EDS) analyses were conducted using a JEOL JSM-6380LA instrument (JEOL Ltd., Japan). Elemental mapping was performed at an accelerating voltage of 15 kV.

2.3.10. ATR-IR spectroscopy

Charred residues obtained from cone calorimeter tests were analysed using infrared spectroscopy. Infrared spectra in the range of 4000–600 cm^{-1} were recorded using a Bruker Tensor 37 Fourier transform infrared (FTIR) spectrometer (Bruker Corporation, USA), equipped with a deuterated triglycine sulfate (DTGS) detector. Measurements were performed in attenuated total reflectance (ATR) mode, which allows direct analysis of solid samples without additional preparation. The spectra were collected with a spectral resolution of 4 cm^{-1} and an accumulation of 32 scans to ensure an adequate signal-to-noise ratio.

2.3.11. Optical measurement

A PerkinElmer Lambda 1050 spectrophotometer (PerkinElmer, Inc., USA) was used to measure the optical reflectance spectra of the samples. It was equipped with a 150 mm integrating sphere, and the reflectance spectra were measured in the wavelength range of 350–800 nm.

3. Results and discussion

3.1. Morphology of rPET foams

As shown in Table 2, the density values of the prepared rPET foam samples range from 240 to 360 kg/m^3, which falls within the expected range for PET foams produced by batch processes [20]. The highest porosity, 82 %, was measured for the foam containing 5 wt% AlPi, whereas the addition of 5 wt% MPP resulted in a lower porosity of 67 %, compared to the 74 % void fraction of the FR-free foam. The observed differences can be attributed to multiple factors, including the particle size and distribution of the additives within the polymer matrix, their effect on melt viscosity, potential cell nucleating behaviour, and chemical interactions with the polymer.

Table 2
Foam density, expansion ratio, and porosity of the foamed samples.

Sample	Foam density [kg/m^3]	Expansion ratio [-]	Porosity [%]
rPET/CE/MMT	339 ± 3	3.9	74
rPET/CE/MMT/AlPi	241 ± 11	5.3	82
rPET/CE/MMT/MPP	411 ± 21	3.1	67
rPET/CE/MMT/AlPi/MPP	354 ± 14	3.6	73

To investigate these effects, SEM images were taken from the cross-section of the rPET foam samples and analyzed. In the SEM micrograph of the FR-free rPET foam (Fig. 1a)), a gradual increase in cell size from the surface to the core is observed, likely due to differences in cooling rates throughout the foam's cross-section. The particles of both flame retardant additives break the homogeneity of the cell structure (Fig. 1b)-d)), indicating poor filler-matrix interaction. Although inherently MPP additive has a smaller particle size (8–20 μm) than AlPi (25–50 μm), noticeably smaller AlPi particles can be observed in the foam's cellular structure. This observation aligns with the findings of *Brehme* et al. [10], who reported rod-like AlPi particles with a median length of 240 nm in injection-moulded poly(butylene terephthalate) (PBT) samples, indicating significant fragmentation of AlPi particles during thermo-mechanical processing. The reduced particle size of AlPi is assumed to play a significant role in achieving improved distribution within the foam structure, thereby enabling higher expansion rates and better overall performance.

The cell sizes were measured manually using the length tool in the AxioVision SE64 Rel. 4.9.1 software. Each cell was evaluated on an SEM image, with 1000–1200 cells per sample. Based on the results, the maximum and minimum cell diameters, as well as the mean, median, standard deviation (SD), and the number of cells larger than 5 μm and 10 μm, were calculated (Table 3). The non-flame-retarded sample exhibited the finest cell structure, with a maximum diameter of 9 μm and the lowest standard deviation of cell diameters. The maximum cell size increased when one or both of the FR additives were used, while the minimum cell size remained approximately the same regardless of the composition (~0.2 μm). However, the number of larger cells was not significant compared to the total number of measured cells, and therefore, the mean value of the flame retarded samples only slightly increased.

The number-weighted diameter, the diameter of a sphere with a volume equal to the mean cell volume, and the polydispersity index of the samples were calculated and are presented Table 4. The polydispersity index of the non-flame-retarded foam was the closest to 1 (1.20), indicating the most homogeneous structure. Among the FR additives, AlPi had the greatest impact on the resulting cell structure, leading to a highly polydisperse morphology. The cell density, defined as the number of cells per cubic centimeter, was determined, too. The highest cell density was achieved in the case of rPET/CE/MMT, which was expected based on its smallest average cell diameter and PD index. The FR-containing foams exhibited cell densities an order of magnitude lower, due to the relatively few but larger cells.

3.2. Thermal characterization of rPET foams

The thermal behaviour of the rPET foams was investigated using TGA. The measured TGA and DTG curves are presented in Fig. 2, while the related data are summarised in Table 5.

Degradation of PET occurs in the range of 380–480 °C in one step, associated with the scission of the ester linkages in the polymer chain. The addition of AlPi did not affect the temperature corresponding to the 5 % weight loss. In contrast, the foam containing MPP exhibited an onset of mass loss approximately 30 °C earlier.

The shoulder-like feature observed on the DTG curve indicates a strong interaction between MPP and PET, and is accompanied by the release of MPP decomposition products, such as ammonia, carbon dioxide, and phosphoric acid [30]. Phosphoric acid readily condenses to form pyrophosphate structures, which can promote the formation of a carbonaceous char. This charring process is also indicated by a reduced degradation rate of the MPP-containing sample. However, the quantity of the residue obtained at 600 °C is the lowest for the rPET/CE/MMT/MPP sample. It was concluded that 5 wt% of MPP is not

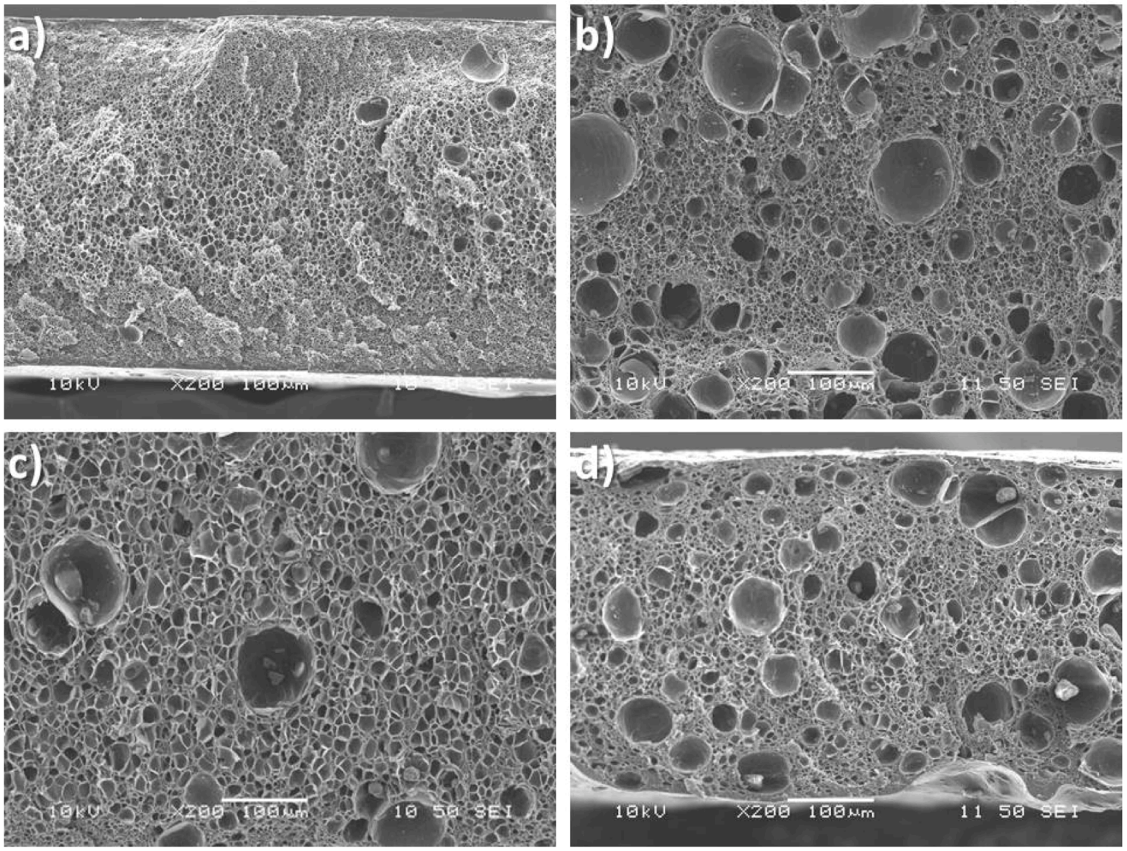

Fig. 1. SEM micrographs of rPET foams with amplification of 200× . a) rPET/CE/MMT; b) rPET/CE/MMT/AlPi; c) rPET/CE/MMT/MPP; and d) rPET/CE/MMT/AlPi/MPP.

Table 3
Cell diameter properties of the foamed samples.

Sample	Maximum [µm]	Minimum [µm]	Mean [µm]	SD [µm]	Median [µm]	>10 µm [%]	>5 µm [%]
rPET/CE/MMT	8.5	0.2	1.6	0.7	1.5	0.0	0.1
rPET/CE/MMT/AlPi	30.8	0.2	1.7	2.4	1.1	1.5	4.9
rPET/CE/MMT/MPP	15.5	0.3	1.8	1.3	1.4	0.2	2.8
rPET/CE/MMT/AlPi/MPP	18.2	0.2	1.8	1.9	1.2	0.9	5.8

Table 4
The cell density, the number-weighted diameter (d_1); the diameter of a sphere with equal volume to the mean cell volume (d_2); and the polydispersity degree (PD) of the foamed samples.

Samples	**Cell density [cells/cm^3]**	**d_1 mean [µm]**	**d_2 mean [µm]**	**PD [-]**
rPET/CE/MMT	$1.26{\cdot}10^{11}$	1.6	1.9	1.20
rPET/CE/MMT/AlPi	$4.47{\cdot}10^{10}$	1.7	4.9	2.85
rPET/CE/MMT/MPP	$3.99{\cdot}10^{10}$	1.8	2.8	1.55
rPET/CE/MMT/AlPi/MPP	$4.44{\cdot}10^{10}$	1.8	3.7	2.07

sufficient to form a considerable amount of charred residue. In contrast, the addition of 5 wt% AlPi increased the amount of residue from 12.5 wt % to 19.2 wt%, indicating significant char-promoting activity and barrier effect of AlPi in PET.

The pronounced shift in decomposition temperature observed for MPP alone was not evident when MPP and AlPi were combined. The decomposition pattern of rPET/CE/MMT/AlPi/MPP closely resembles that of rPET/CE/MMT/AlPi, indicating that the main decomposition steps are largely governed by AlPi. A similar trend was observed by *Braun* et al. [31], who investigated the decomposition behavior of AlPi and MPP, both individually and in combination, in glass-fiber-reinforced PA 6.6 composites. They suggested that, when MPP is used in combination with AlPi, the Lewis acid activity of the phosphate is suppressed due to the formation of aluminium phosphate.

DSC analyses were conducted to investigate the phase structure and thermal transitions of the rPET foams. As shown in Table 6, the crystalline ratio, determined from the first heating scan, ranged between 31 % and 35 % for all foam samples. This degree of crystallinity is typical for foamed PET systems processed above the glass transition temperature (T_g), where crystallization is enhanced by chain orientation that occurs during cell growth [32]. High crystallinity typically results in improved stiffness and better thermomechanical performance [20]. In flame-retarded foams, the crystallization peak shifts to higher temperatures during cooling compared to the FR-free reference, indicating a

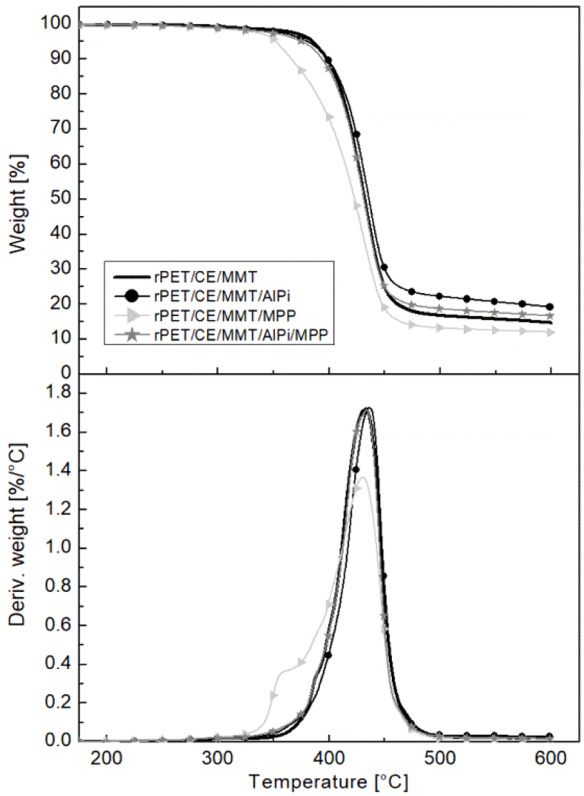

Fig. 2. TGA and DTG curves of rPET foams.

Table 5
Thermal characteristics of rPET foams.

Sample	5 % weight loss [°C]	Maximum degradation speed [%/ °C]	Temperature of maximum degradation speed [°C]	Residue at 600 °C [wt%]
rPET/CE/MMT	383.5	1.69	431.9	12.5
rPET/CE/MMT/AlPi	381.0	1.77	436.2	19.2
rPET/CE/MMT/MPP	352.4	1.39	430.2	12.0
rPET/CE/MMT/AlPi/MPP	375.3	1.74	433.6	16.7

nucleating effect of the incorporated flame retardants. Among the studied FRs, MPP showed a more pronounced promotion of crystallization. However, this effect may also be partially attributed to a reduction in molecular weight in the presence of MPP, which can enhance chain mobility and facilitate crystallization [19]. Additionally, the presence of MMT may contribute as a heterogeneous nucleating agent in these systems, further influencing the crystallization behaviour.

3.3. Flame retardancy of rPET samples

The LOI values of the flame-retardant-containing rPET foams are summarised in Table 7. The LOI of the rPET foam increased from 19.0 % to 25.0 % by adding 5 wt% of AlPi, while the rPET foams with 5 wt% MPP and the combined additive system reached only lower LOI values of 22.5 % and 21.5 %, respectively. This result may be attributed to the higher phosphorus content in the AlPi-containing samples at an identical additive ratio of 5 wt% (see Table 1), but it also indicates that the gas-phase mechanism is more effective in reducing the flammability of the rPET foams. The decreased LOI measured for the rPET/CE/MMT/AlPi/MPP sample suggests an antagonistic interaction between the two phosphorus-based additives in the system.

The flammability performance of the foam samples was also investigated using the PCFC method. According to the results presented in Table 8, MPP was more effective in lowering the FGC and pHRR,

Table 6
Results of DSC analysis of rPET foams.

Sample	Melting temperature[a] [°C]	Crystallinity[a] [%]	Cooling crystallization peak[b] [°C]	Glass transition temperature[c] [°C]	Crystallinity[c] [%]
rPET/CE/MMT	248.2	33.7	194.3	79.4	24.0
rPET/CE/MMT/AlPi	249.7	35.1	198.7	76.8	27.6
rPET/CE/MMT/MPP	248.0	31.3	205.9	76.7	25.5
rPET/CE/MMT/AlPi/MPP	247.2	34.5	205.5	77.3	26.2

[a] first DSC run (heating);.
[b] second DSC run (cooling);.
[c] third DSC run (heating).

Table 7
The LOI values of the foamed samples.

Sample	LOI [%]
rPET/CE/MMT	19.0
rPET/CE/MMT/AlPi	25.0
rPET/CE/MMT/MPP	22.5
rPET/CE/MMT/AlPi/MPP	21.5

Table 8
PCFC results of the foamed samples.

Sample	FGC [J/gK]	pHRR [W/g]	T_p [°C]	THR [kJ/g]	Residual mass [wt%]
rPET/CE/MMT	258.4	407	456	15.7	11.9
rPET/CE/MMT/AlPi	260.0	409	454	15.9	16.3
rPET/CE/MMT/MPP	219.9	254	439	18.2	12.4
rPET/CE/MMT/AlPi/MPP	256.5	387	449	16.5	15.7

reflecting better suppression of fire behavior in the early stages of fire development, whereas AlPi contributed more significantly to increasing the residual mass. The THR of the MPP-containing foam samples increased relative to the FR-free reference. This behaviour correlates with the observed lowering of the PET decomposition temperature in the presence of MPP (Fig. 2), which is attributed to the release of acidic phosphorus species during MPP degradation. At lower temperatures, these acids catalyze ester bond scission, generating lower-molecular-weight fragments that volatilize more readily [13]. Consequently, a larger quantity of combustible gases is released during the early stages of heating, while producing less solid residue capable of acting as a protective barrier. At higher temperatures, the same phosphorus-derived acids promote dehydration and crosslinking reactions, leading to the formation of a phosphorus-rich char [33]. This char enhances condensed-phase flame retardancy by acting as a protective barrier, thereby limiting further polymer decomposition and heat release. In PCFC measurements, the combined use of both additives led to intermediate performance with respect to the analysed parameters. However, the resulting HRR curve is more similar to that observed for the rPET/CE/MMT/AlPi foam sample. This suggests that the presence of AlPi moderates the decomposition-temperature shift typically induced by MPP, thereby influencing the overall combustion behaviour of the system.

Heat release rate, mass loss, and smoke production rate curves of the foamed rPET samples, obtained during cone calorimetric tests, are presented in Fig. 3, and corresponding data are summarised in Table 9. It can be seen that AlPi, being mostly active in the gas phase but also showing condensed-phase activity, noticeably increased the TTI and reduced the pHRR and THR compared to the FR-free reference, and contributed to the formation of a significant (20 %) amount of char, accompanied by moderate smoke emission. This result suggests that part of the phosphorus of AlPi remains in the condensed phase and induces char formation. Near the end of the burning process, a second peak appeared in the corresponding HRR curve, likely due to the decomposition of the carbonaceous heat-protective shield as the underlying

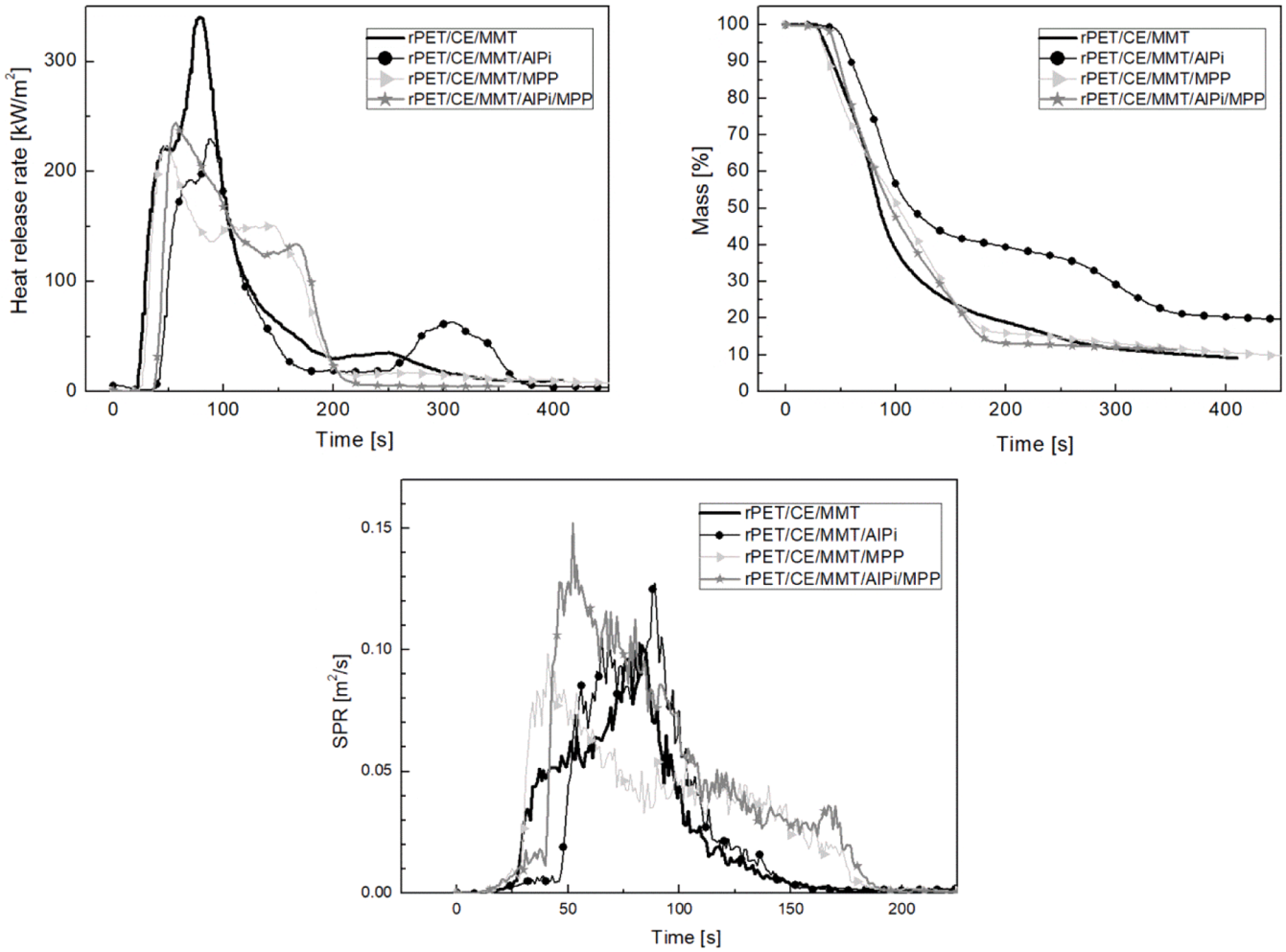

Fig. 3. a) Heat release rate; b) mass loss, and c) smoke production rate of foamed rPET samples during cone calorimetric analysis.

Table 9
Cone calorimetry test results of the foamed samples.

Sample	TTI [s]	pHRR [kW/m^2]	t_{pHRR} [s]	THR [MJ/m^2]	MARHE [kW/m^2]	EHC [MJ/kg]	Residual mass [wt%]	TSP [m^2/m^2]	FRI [-]
rPET/CE/MMT	23	341	78	29.2	177	18.8	9.1	614	-
rPET/CE/MMT/AlPi	41	230	88	22.5	107	16.6	20.0	717	3.4
rPET/CE/MMT/MPP	27	224	47	27.3	129	17.8	9.7	773	1.9
rPET/CE/MMT/AlPi/MPP	39	244	57	24.4	125	16.3	12.2	1031	2.8

Table 10
Quantitative assessment of the three flame-retardant effects.

Sample	Flame-inhibition effect [%]	Barrier and protective effect [%]	Charring effect [%]
rPET/CE/MMT/AlPi	12.0	12.5	12.0
rPET/CE/MMT/MPP	5.3	29.7	0.7
rPET/CE/MMT/AlPi/MPP	13.5	14.4	3.4

material reached the pyrolysis zone. The condensed-phase activity of MPP (charring) is reflected in the broadened shape of the HRR curve and the significantly (by 35 %) reduced pHRR value characteristic of the rPET/CE/MMT/MPP sample. Interestingly, however, the amount of combustion residue has not noticeably increased. This observation aligns with the moderate increase in residual mass observed for MPP-containing rPET foam samples in both TGA (Table 5) and PCFC analyses (Table 8). The rPET foam containing both AlPi and MPP exhibited intermediate fire performance compared to the foams containing AlPi or MPP alone. However, this sample showed the highest total smoke production, further confirming the disadvantageous effect of this additive combination. The highest FRI value of 3.4 was calculated for the sample containing 5 wt% AlPi, highlighting the effective flame-retardant action of AlPi in rPET foams.

The three flame-retardant effects, as proposed by *Brehme* et al. [34], were assessed quantitatively as well. The results are summarised in Table 10. AlPi was found to exhibit a balanced combination of flame inhibition, barrier formation, and charring effects. This observation aligns with the findings of *Braun* et al. [11], which indicate that, in addition to flame inhibition, the primary flame-retardant mechanism of AlPi is the formation of an effective barrier of aluminium phosphates. In the case of MPP, the dominant barrier effect is accompanied by a low charring effect, suggesting that the material initially resists burning by forming a physical barrier but does not contribute to the formation of a self-extinguishing char layer that could further inhibit combustion, presumably due to insufficient thermal stability.

The quantity and morphology of the charred residues from the cone calorimeter test can be observed from the digital images presented in Fig. 4. After the fire test, a large portion of the alumina sample holder is still covered by the char formed from the AlPi-containing rPET foam. In contrast, the residues remaining after combustion of the MPP-containing foams do not create a coherent surface.

EDS analysis of the combustion residues, shown in Table 11, revealed that the char formed from the MPP-containing rPET foam is carbon-rich, whereas the char from the AlPi-containing sample exhibits high aluminium and phosphorus content. Such a phospho-carbonaceous char is considered to be thermally more stable than a conventional poly-aromatic char [35].

The chemical structure of the combustion residues was investigated using ATR-IR spectroscopy; the gained spectra are presented in Fig. 5. The absorption vibrations of the $C = O$ and C–O–C functional groups

Table 11
Elemental composition (EDS data) of the combustion residues.

Sample	C [wt%]	O [wt%]	Al [wt%]	Si [wt%]	P [wt%]
rPET/CE/MMT	78.4	19.1	0.5	2.0	0.0
rPET/CE/MMT/AlPi	37.5	41.2	8.5	1.6	11.2
rPET/CE/MMT/MPP	69.3	25.6	0.4	0.7	4.0
rPET/CE/MMT/AlPi/MPP	56.6	32.3	3.4	1.9	5.8

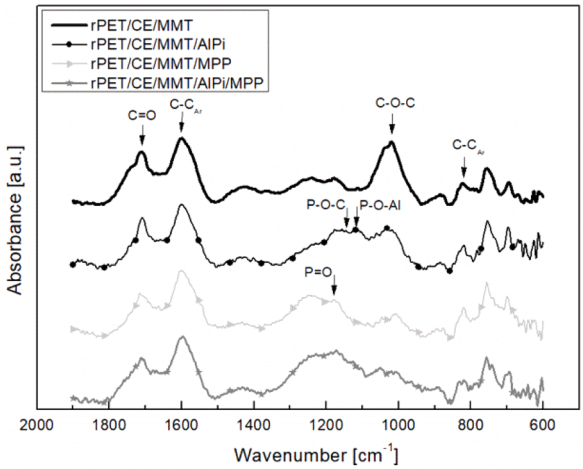

Fig. 5. ATR-FTIR spectra of char residues after cone calorimeter tests.

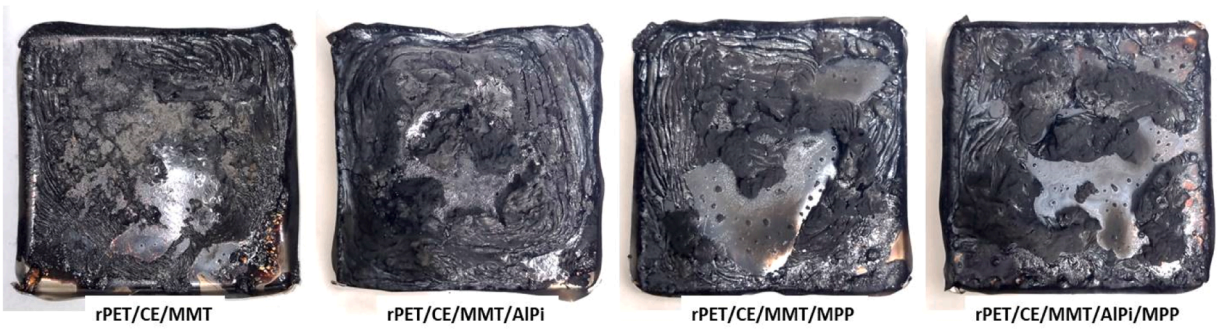

Fig. 4. Images of char residues obtained from cone calorimeter tests.

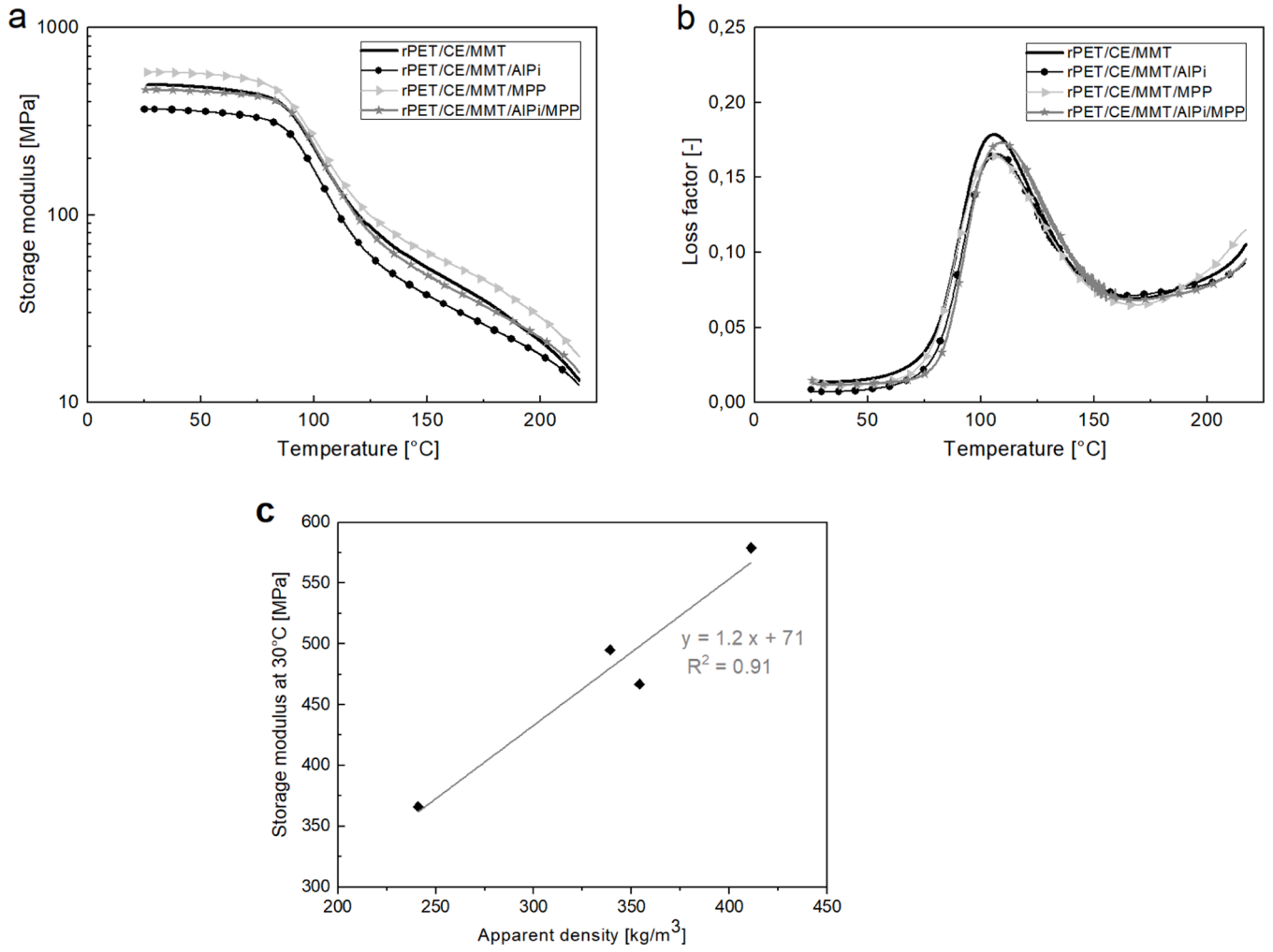

Fig. 6. a) Storage modulus and b) loss factor of flame retarded rPET foamed samples as a function of temperature; c) correlation between storage modulus and foam density.

associated with PET appear in all spectra at 1710 cm^{-1} and 1021 cm^{-1}, respectively. The polyaromatic structure of the chars is evidenced by the characteristic C–C_{Ar} vibrations observed at 1597 cm^{-1} and 820 cm^{-1}. The presence of phosphorus-containing moieties in the residues from FR-containing foams is indicated by additional vibration bands corresponding to $P = O$ at 1215 cm^{-1} and P–O–C at 1150 cm^{-1}. These findings confirm that the char residues formed from FR-containing rPET foams consist of polyaromatic structures linked with phospho-carbonaceous networks via P–O–C linkages. In the case of the char formed from the rPET foam containing 5 wt% AlPi, the band at 1100 cm^{-1} is attributed to the asymmetric P–O–Al stretching vibration, confirming the presence of aluminium phosphates in the residue. These compounds can act as effective barriers against heat and fuel transport [11], and are therefore considered to significantly contribute to the improved fire-retardant performance of the AlPi-containing rPET foams.

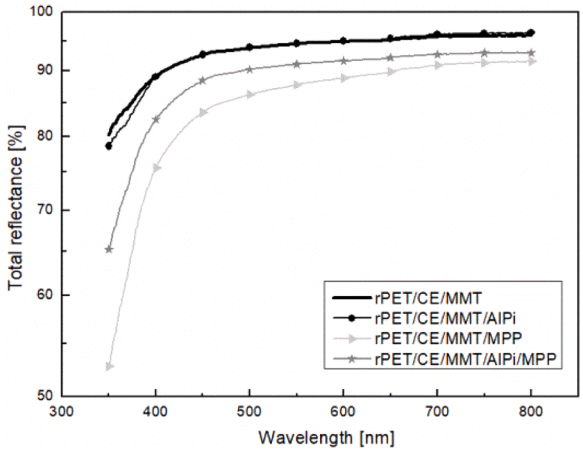

Fig. 7. Total reflectance of the rPET foams across the visible light range.

3.4. Applicability

To support potential applications, additional properties of the manufactured flame-retarded rPET foams were investigated.

3.4.1. Heat stability

The thermo-mechanical behaviour of the foams was assessed using dynamic mechanical analysis (DMA). The recorded storage modulus and loss factor curves are presented in Fig. 6a and b, respectively. At room temperature, the storage modulus of the foam samples ranges from 360 to 580 MPa and remains relatively stable up to 85 °C. Even at 100 °C, the foams maintain a storage modulus above 200 MPa, demonstrating good mechanical integrity at elevated temperatures. In general, foam mechanical properties are expected to improve as density increases [19,36,37]. Accordingly, the storage modulus of the investigated foam samples

was found to depend primarily on their apparent density, which showed an approximately linear correlation within the examined range (Fig. 6c), while composition had a comparatively minor influence.

The glass transition temperature (T_g), generally considered the upper limit for practical applicability, was determined by the peak in the loss factor and found to range between 104 and 109 °C, depending on the foam composition. This represents an approximate 45 °C increase compared to the T_g of unfoamed, highly amorphous PET, which is around 65 °C. These results are consistent with the DSC data shown in Table 6 and suggest that the highly crystalline structure of the rPET foams contributes to their enhanced heat stability. Consequently, these foams are well-suited for applications requiring increased heat resistance.

3.4.2. Optical characteristics

Despite being produced from greyish-colored recycled tray flakes, the microcellular foams appear snow-white, suggesting enhanced light-reflecting properties. Indeed, reflectance measurements confirmed high reflectivity in the visible light range. As shown in Fig. 7, the total reflectance of the prepared foams, measured using an integrating sphere, represents the overall amount of light reflected across the visible spectrum (400–800 nm). As the wavelength approaches the near-infrared region, even the flame-retarded foams exhibit a total reflectance above 90 %.

The incorporation of AlPi particles had a negligible effect on the total reflectance within the examined wavelength range, while the addition of MPP was found to slightly reduce this optical property. Since nearly 95 % of solar radiation lies within the 400–2500 nm range, the observed high reflectivity in the visible and near-IR spectra significantly reduces solar heat gain, contributing to lower material temperatures under sunlight (passive cooling). Combined with the material's reduced thermal conductivity, the prominent light-reflecting properties suggest that the prepared foams possess high thermal insulating efficiency, making them promising candidates for use in building materials. Furthermore, the high optical reflectivity, along with enhanced fire resistance, broadens their potential application in fields such as lighting and optical systems, as well as in solar energy technologies.

4. Conclusions

This study demonstrates that AlPi, a primarily gas-phase active flame retardant, provides superior fire performance in rPET foams compared to the predominantly condensed-phase active MPP. No synergistic enhancement was observed when AlPi and MPP were combined. The pronounced effectiveness of AlPi at low loadings is attributed not only to its gas-phase flame inhibition but also to the formation of a thermally stable char layer enriched with aluminium phosphates, which contributes to enhanced thermal stability.

The CO_2-assisted batch foaming process enabled the production of low-density, microcellular rPET foams with desirable multifunctional properties. These foams exhibit excellent flame retardancy with low thermal conductivity, high mechanical and heat resistance, and outstanding light reflectance, which contributes to reduced solar heat gain (passive cooling). Additionally, they are expected to provide sound- and vibration dampening capabilities. Owing to this combination of properties, the developed flame-retardant rPET foams show high potential for use in construction, transportation, and solar energy applications.

CRediT authorship contribution statement

Kata Enikő Decsov: Writing – review & editing, Writing – original draft, Visualization, Validation, Methodology, Investigation, Formal analysis, Data curation, Conceptualization. **Emese Győry-Slezák:** Writing – review & editing, Investigation, Formal analysis. **Dániel Gere:** Writing – review & editing, Validation, Resources, Methodology, Funding acquisition. **Ferenc Ronkay:** Writing – review & editing, Validation, Supervision, Resources, Project administration, Methodology, Funding acquisition, Data curation. **Béla Botond Marosfői:** Writing – review & editing, Supervision, Resources, Investigation. **Sándor Lenk:** Writing – review & editing, Resources, Investigation, Formal analysis. **Katalin Bocz:** Writing – review & editing, Writing – original draft, Visualization, Validation, Supervision, Resources, Project administration, Methodology, Funding acquisition, Data curation, Conceptualization.

Declaration of competing interest

The authors declare that they have no known competing financial interests or personal relationships that could have appeared to influence the work reported in this paper.

Acknowledgement

The project was funded by the National Research, Development and Innovation Fund of Hungary in the frame of the 2018–1.3.1-VKE-2018–00017 project. The research was funded by the Sustainable Development and Technologies National Programme of the Hungarian Academy of Sciences (FFT NP FTA). The research was funded by the Hungarian Scientific Research Fund, grant number PD146135 and K143039. E. Győry-Slezák expresses her gratitude for the project no KDP-IKT-2023–900-I1–00000957/0000003, which has been implemented with the support provided by the Ministry of Culture and Innovation of Hungary from the National Research, Development and Innovation Fund, financed under the KDP-2023 funding scheme. Dániel Gere and Sándor Lenk are thankful for the János Bolyai Research Scholarship (grant number: BO/00894/23/6 and BO/00038/23, respectively) of the Hungarian Academy of Sciences. The authors are thankful to Mr. Balázs Pinke for his help in the DMA tests.

Data availability

Data will be made available on request.

References

[1] K. Bocz, B. Molnár, G. Marosi, F. Ronkay, Preparation of low-density microcellular foams from recycled PET modified by solid State polymerization and chain extension, J. Polym. Environ. 27 (2019) 343–351, https://doi.org/10.1007/s10924-018-1351-z.

[2] L. Di Maio, I. Coccorullo, S. Montesano, L. Incarnato, Chain extension and foaming of recycled PET in extrusion equipment, Macromol. Symp. 228 (2005) 185–200, https://doi.org/10.1002/masy.200551017.

[3] C.-C. Lai, C.-T. Yu, F.-M. Wang, H.-T. Hsiao, W.-C. Liang, Y.-H. Ho, W.-F. Teng, L.-C. Liu, C.-M. Chen, Preparation of recycled polyethylene terephthalate composite foams and their feasible evaluation for electronic packages, Polym. Test. 74 (2019) 1–6, https://doi.org/10.1016/j.polymertesting.2018.12.009.

[4] I. Coccorullo, L. Di Maio, S. Montesano, L. Incarnato, Theoretical and experimental study of foaming process with chain extended recycled PET, Express. Polym. Lett. 3 (2009) 84–96, https://doi.org/10.3144/expresspolymlett.2009.12.

[5] K. Bocz, F. Ronkay, B. Molnár, D. Vadas, M. Gyürkés, D. Gere, G. Marosi, T. Czigany, Recycled PET foaming: supercritical carbon dioxide assisted extrusion with real-time quality monitoring, Adv. Ind. Eng. Poly. Res. 4 (2021) 178–186, https://doi.org/10.1016/j.aiepr.2021.03.002.

[6] S.V. Levchik, E.D. Weil, Flame retardancy of thermoplastic polyester - a review of the recent literature, Polym. Int. 54 (2005) 11–35, https://doi.org/10.1002/pi.1663.

[7] B. Xu, M. Jia, D. Wang, S. Zhao, S. Zhu, L. Qian, A discovery for phosphorus valence and unsaturated bonds in polyphosphate/polyphosphonate: promotion or inhibition for its flame-retardant mode of action in PET, Polym. Degrad. Stab. 227 (2024), https://doi.org/10.1016/j.polymdegradstab.2024.110873.

[8] U. Braun, A.I. Balabanovich, B. Schartel, U. Knoll, J. Artner, M. Ciesielski, M. Döring, R. Perez, J.K.W. Sandler, V. Altstädt, T. Hoffmann, D. Pospiech, Influence of the oxidation state of phosphorus on the decomposition and fire behaviour of flame-retarded epoxy resin composites, Polymer 47 (2006) 8495–8508, https://doi.org/10.1016/j.polymer.2006.10.022.

[9] D. Goedderz, L. Weber, D. Markert, A. Schießer, C. Fasel, R. Riedel, V. Altstädt, C. Bethke, O. Fuhr, F. Puchtler, J. Breu, M. Döring, Flame retardant polyester by combination of organophosphorus compounds and an NOR radical forming agent, J. Appl. Polym. Sci. 137 (2020), https://doi.org/10.1002/app.47876.

[10] S. Brehme, T. Köppl, B. Schartel, V. Altstädt, Competition in aluminium phosphinate-based halogen-free flame retardancy of poly(butylenes terephthalate) and its glass-fibre composites, E-Polym. 14 (2014) 193–208, https://doi.org/10.1515/epoly-2014-0029.
[11] U. Braun, B. Schartel, Flame retardancy mechanisms of aluminium phosphinate in combination with melamine cyanurate in glass-fibre-reinforced poly(1,4-butylene terephthalate), Macromol. Mater. Eng. 293 (2008) 206–217, https://doi.org/10.1002/mame.200700330.
[12] J. Li, Z. Qin, C. Zhai, R. Yang, Study on the synergistic flame-retardancy of phenyl/vinyl silicones quioxane and aluminum diethyl phosphinate on polyethylene terephthalate, Polym. Degrad. Stab. 220 (2024), https://doi.org/10.1016/j.polymdegradstab.2024.110660.
[13] T. Li, S. Li, T. Ma, Y. Zhong, L. Zhang, H. Xu, B. Wang, X. Sui, X. Feng, Z. Chen, Z. Mao, Flame-retardant poly (ethylene terephthalate) enabled by a novel melamine polyphosphate nanowire, Polym. Adv. Technol. 31 (2020) 795–806, https://doi.org/10.1002/pat.4815.
[14] A. Ramani, A.E. Dahoe, On flame retardancy in polycaprolactam composites by aluminium diethylphosphinate and melamine polyphosphate in conjunction with organically modified montmorillonite nanoclay, Polym. Degrad. Stab. 105 (2014) 1–11, https://doi.org/10.1016/j.polymdegradstab.2014.03.020.
[15] N.A. Isitman, M. Dogan, E. Bayramli, C. Kaynak, The role of nanoparticle geometry in flame retardancy of polylactide nanocomposites containing aluminium phosphinate, Polym. Degrad. Stab. 97 (2012) 1285–1296, https://doi.org/10.1016/j.polymdegradstab.2012.05.028.
[16] A. Ramani, A.E. Dahoe, On the performance and mechanism of brominated and halogen free flame retardants in formulations of glass fibre reinforced poly (butylene terephthalate), Polym. Degrad. Stab. 104 (2014) 71–86, https://doi.org/10.1016/j.polymdegradstab.2014.03.021.
[17] W. Tabaka, B. Schartel, Less is more: optimised fire performance in glass fibre-reinforced polybutylene terephthalate laminates with concentrated flame retardant top layer, Compos., C: Open Access. 16 (2025) 100577, https://doi.org/10.1016/j.jcomc.2025.100577.
[18] C. Bethke, D. Goedderz, L. Weber, T. Standau, M. Döring, V. Altstädt, Improving the flame-retardant property of bottle-grade PET foam made by reactive foam extrusion, J. Appl. Polym. Sci. 137 (2020), https://doi.org/10.1002/app.49042.
[19] K. Bocz, F. Ronkay, D. Vadas, B. Molnár, D. Gere, T. Czigány, G. Marosi, Flame retardancy of PET foams manufactured from bottle waste, J. Therm. Anal. Calorim. 148 (2023) 217–228, https://doi.org/10.1007/s10973-022-11423-3.
[20] N. Lukács, F. Ronkay, B. Molnár, B. Marosfői, K. Bocz, Characterisation of flame retarded recycled PET foams produced by batch foaming, Polym. Test. 124 (2023), https://doi.org/10.1016/j.polymertesting.2023.108104.
[21] J. Wang, Q. Ren, W. Zheng, W. Zhai, Improved flame-retardant properties of poly (lactic acid) foams using starch as a natural charring agent, Ind. Eng. Chem. Res. 53 (2014) 1422–1430, https://doi.org/10.1021/ie403041h.
[22] D. Vadas, T. Igricz, J. Sarazin, S. Bourbigot, G. Marosi, K. Bocz, Flame retardancy of microcellular poly(lactic acid) foams prepared by supercritical CO2-assisted extrusion, Polym. Degrad. Stab. 153 (2018) 100–108, https://doi.org/10.1016/j.polymdegradstab.2018.04.021.
[23] K. Wang, J. Wang, D. Zhao, W. Zhai, Preparation of microcellular poly(lactic acid) composites foams with improved flame retardancy, J. Cell Plast. 53 (2017) 45–63, https://doi.org/10.1177/0021955X16633644.
[24] F. Ronkay, B. Molnár, F. Szalay, D. Nagy, B. Bodzay, I.E. Sajó, K. Bocz, Development of flame-retarded nanocomposites from recycled PET bottles for the electronics industry, Polymers 11 (2019) 233, https://doi.org/10.3390/polym11020233.
[25] V. Langlois, C.T. Nguyen, F. Detrez, J. Guilleminot, C. Perrot, Permeability of polydisperse solid foams, Phys. Rev. E 105 (2022) 015101, https://doi.org/10.1103/PhysRevE.105.015101.
[26] J.D. Badia, E. Strömberg, S. Karlsson, A. Ribes-Greus, The role of crystalline, mobile amorphous and rigid amorphous fractions in the performance of recycled poly (ethylene terephthalate) (PET), Polym. Degrad. Stab. 97 (2012) 98–107, https://doi.org/10.1016/j.polymdegradstab.2011.10.008.
[27] R.E. Lyon, N. Safronava, S. Crowley, R.N. Walters, A molecular-level fire growth parameter, Polym. Degrad. Stab. 186 (2021), https://doi.org/10.1016/j.polymdegradstab.2020.109478.
[28] H. Vahabi, E. Movahedifar, B.K. Kandola, M.R. Saeb, Flame Retardancy Index (FRI) for polymer materials ranking, Polymers 15 (2023) 2422, https://doi.org/10.3390/polym15112422.
[29] W. Yan, J. Yu, M. Zhang, T. Wang, C. Wen, S. Qin, W. Huang, Effect of multiwalled carbon nanotubes and phenethyl-bridged DOPO derivative on flame retardancy of epoxy resin, J. Polym. Res. 25 (2018) 72, https://doi.org/10.1007/s10965-018-1472-z.
[30] T.H. Nguyen, D.Q. Hoang, J. Kim, Effect of ammonium polyphosphate and melamine pyrophosphate on fire behavior and thermal stability of unsaturated polyester synthesized from poly(ethylene terephthalate) waste, Macromol. Res. 26 (2018) 22–28, https://doi.org/10.1007/s13233-018-6004-5.
[31] U. Braun, B. Schartel, M.A. Fichera, C. Jäger, Flame retardancy mechanisms of aluminium phosphinate in combination with melamine polyphosphate and zinc borate in glass-fibre reinforced polyamide 6,6, Polym. Degrad. Stab. 92 (2007) 1528–1545, https://doi.org/10.1016/j.polymdegradstab.2007.05.007.
[32] T. Standau, C. Zhao, S.M. Castellón, C. Bonten, V. Altstädt, Chemical modification and foam processing of polylactide (PLA), Polymers 11 (2019), https://doi.org/10.3390/polym11020306.
[33] S. Zhao, B. Xu, H. Shan, Q. Zhang, X. Wang, How do phosphorus compounds with different valence states affect the flame retardancy of PET? Polymers 15 (2023) https://doi.org/10.3390/polym15081917.
[34] S. Brehme, B. Schartel, J. Goebbels, O. Fischer, D. Pospiech, Y. Bykov, M. Döring, Phosphorus polyester versus aluminium phosphinate in poly(butylene terephthalate) (PBT): flame retardancy performance and mechanisms, Polym. Degrad. Stab. 96 (2011) 875–884, https://doi.org/10.1016/j.polymdegradstab.2011.01.035.
[35] S.V. Levchik, E.D. Weil, Thermal decomposition, combustion and fire-retardancy of polyurethanes - a review of the recent literature, Polym. Int. 53 (2004) 1585–1610, https://doi.org/10.1002/pi.1314.
[36] Z. Zhang, C. Xin, C. Ma, W. Xu, F. Ren, Y. He, Morphology and compressive properties of extruded polyethylene terephthalate foam, Polymers 16 (2024) 776, https://doi.org/10.3390/polym16060776.
[37] L. Santo, D. Bellisario, F. Quadrini, Shape memory behavior of PET foams, Polymers 10 (2018), https://doi.org/10.3390/polym10020115.